Development of Image Reconstruction Technology for Ultra High-resolution PET and Micron-CT

IV. 3. Development of Image Reconstruction Technology for Ultra High-resolution PET and Micron-CT

Yamaguchi T., Ishii K., Yamazaki H., Matsuyama S., Kikuchi Y., Momose G., YamamotoY., and Watanabe Y.

Department of Quantum Science and Energy Engineering, Tohoku University

ABSTRACT

The development of high spatial resolution PET is vital for testing new medicines on small animals. We are developing "Dual Head PET" with high resolution and high sensitivity, whose detectors are in two arrays facing each other. The "Dual Head PET" provides incomplete projection data and the FBP algorithm is not suitable. On the other hand, a prototype of Micron-CT for biological research is being developed at Tohoku University. This Micron-CT uses a point X-ray source with a spot size of 3 μm and an X-ray CCD with 1000×1000 pixels of 8 μm×8 μm, achieving spatial resolutions of the order of micro-meter. The event data obtained by the X-ray CCD is statistically poor at practicable scanning time and the 3D FBP algorithm is not suitable because it is highly sensitive to statistical noise. Hence, we applied the Expectation-Maximization (EM) algorithm for image reconstruction and developed an image reconstruction method for Dual Head PET and Micron-CT. We demonstrated PET ant CT images, which were reconstructed the simulated data measured with Dual Head PET and the experimental data measured with Micron-CT.

INTRODUCTION

X-ray CT (Computed Tomography) was invented by G. Hounsfield and J. Ambrose in 1979. Now, a Cone-beam is being used for CT scan. After the invention of the CT scanner, Filtered Back Projection (FBP) algorithm incorporated into an analytical technique is usually used as the main method for the image reconstruction algorithm. For image reconstruction method with cone-beam, the Feldkamp method[1)] is widely used now. This is FBP weighted by taking into account the cone angle. On the other hand, an algebraic

technique was devised for the image reconstruction method. The algebraic technique in Positron emission tomography has been widely studied since Shepp and Vardi[2] developed a method based on expectation maximization (EM) algorithm. K. Lange and R. Carson applied the EM algorithm to X-ray CT[3]. In comparison with FBP, the Signal-to-Noise ratio of images could be improved considerably. However, EM method has two disadvantages. Firstly, it is time consuming and secondly when projection data include noise, the solution diverges as the EM iterative procedure is implemented. To overcome the first disadvantage, acceleration methods to reduce the computational time have been proposed and the recent trend focuses on the use of block-iterative methods. One acceleration method is the ordered subsets (OS) EM algorithm (Hudson and Larkin[4]). In OSEM, projection data are grouped into a number of subsets, and the EM iterative procedure is repeatedly adopted for each subset until all subsets have been processed. To resolve the second shortcoming, various stopping rules are proposed. For instance, cross validation algorithm was used as a stopping rule[5]. In this algorithm, the projection data is divided into two groups and EM algorithm is applied to one data set. The Poisson likelihood of the reconstructed image is calculated with the other data set. When it is maximized, the EM iteration is stopped. The other stopping rule is Kontaxakis's stopping rule[6]. This rule stops the EM iteration when the image updating remains a constant. Maximum '*A posteriori*' (MAP) algorithm was devised as the image reconstruction method to stabilize EM reconstructed images with priori information for images[7]. When a projection data set is acquired, this method finds a solution that maximizes the conditional probability on images. This solution converges when the iteration number is increased. Considering poor statistical accuracy in X-ray CCD data obtained by practicable data acquisition time, hence, we applied the EM algorithm for image reconstruction to Micron-CT. To reduce computation time, OSEM algorithm was applied to the image reconstruction.

Meanwhile, research activity in PET instrumentation is largely dedicated to obtaining high spatial image resolution[8,9]. When the spatial resolution is better than 1mm, several resolution-limiting factors have to be taken into account in order to achieve the desired intrinsic resolution. These are essentially detector size, angular deviation and positron range. The influence of positron range is ignored here since the FWHM of the positron distribution is less than 0.2mm for ^{18}F-labeled radiopharmaceuticals. A scintillator detector is realized a limitation of miniaturizing it, so a thin Semiconductor detector improves the spatial resolution degradation caused by detector size. The solution for avoiding the degrading effect

of angular deviation lies in shortening the distance between opposite detector rows. In order to achieve high spatial resolution images, we are developing "Dual Head PET" by arranging a thin CdTe in two rows facing each other at short distance. This detector arrangement allows to reduce the effect of angular deviation and increases the overall scanner sensitivity. EM and MAP algorithm was chosen to reconstruct the data sets measured by Dual Head PET. In addition, Depth of Interaction (DOI) information improves the degradation of spatial resolution caused by parallax error, so that it is programmed in process of the reconstruction.

MATERIALS AND METHODS

For Dual Head PET, *Maximum A Posteriori* (MAP) algorithm is applied to the image reconstruction to improve reconstructed images[10-12]. MAP can remove the divergence in quantitative accuracy at higher iteration numbers often seen in EM due to noise. MAP updates the voxel value $\lambda_b{}^n$ by

$$\lambda_b{}^{n+1} = \frac{\lambda_b{}^n}{\sum_{d=1}^{D} p_{bd}\left(1+\frac{1}{\beta}\frac{\partial U\left(\lambda_b{}^n\right)}{\partial \lambda_b{}^n}\right)} \sum_{d=1}^{D} \frac{n_d p_{bd}}{\sum_{k=1}^{B} \lambda_k{}^n p_{kd}} \qquad (1)$$

where p_{bd} is the probability that γ-rays generating in the *b*th voxel are measured with the *d*th detector pair, n_d indicates the detected event in the *d*th detector pair,

$$\frac{\partial U\left(\lambda_b{}^n\right)}{\partial \lambda_b{}^n} = \sum_{l\in N_b} \varpi_{bl} \frac{\partial V(r,\delta)}{\partial r} = \sum_{l\in N_b} \varpi_{bl} \frac{16(r/\delta)}{\left(3+(r/\delta)^2\right)^2} \qquad (2)$$

and N_b is "cliques" which are defined by voxel *b* and voxels *l* next to *b*. The clique energy $V(r,\delta)$ is a function of the difference *r* between the values of two voxels *b* and *l*. The constant ω_{bl} is a weighting factor between voxels *b* and *l*. The parameter δ controls the effect of the energy function, and parameter δ determines the location of the derivative energy function peak with respect to *r*. In this study, the values of ω_{bl} were fixed at 1 and the value of δ was set to 100. When the parameter δ is kept constant during reconstruction, MAP has a noise-suppression effect on only one region. We assumed that voxel values followed a Poisson distribution. Hence the parameter δ was set to $2\sigma = 2\sqrt{voxelvalue}$. We compared the image with MAP (δ=*const*) algorithm and that of MAP (δ=*variable*).

For Micron-CT, Gradient algorithm is applied, which belongs to the group of EM methods. Gradient algorithm updates the voxel value μ_j^n by;

$$\mu_j^{n+1} = \mu_j^n \cdot \frac{\sum_{i=1}^{I} d_i \cdot \exp\left(-\sum_{j=1}^{J} l_{ij} \cdot \mu_j^n\right) \cdot l_{ij}}{\sum_{i=1}^{I} y_i \cdot l_{ij}} \qquad (3)$$

where l_{ij} is the intersection length for X-rays passing through the *j*th voxel in the *i*th projection, y_i is the number of detected events for the *i*th projection and d_i is the expected number of photon counts emerging from the source along the *i*th projection. l_{ij} is weighted to be able to reconstruct a 3D object with the incomplete data.

Figure 1 shows the simulation geometry of Dual Head PET. Monte Carlo method is used in order to simulate coincidence data sets for a pair of Dual Head PET. The measurement is simulated with 32 CdTe-crystals in 2 layers that is 4 arrays of 1.2×1.2×3 mm^3. The distance between detector arrays is 50 mm. Figure 2 shows digital phantoms. Phantom 1 consists of an uniform disc and two circular hot areas. The warm background and the hot discs have relative emision activities of 1 and 5, and diameters of 30 mm and 6 mm, respectively. Phantom 1 has 0.2 M total counts. Phantom 2 consists of an uniform disc, a lower right cold disc, two circular hot areas and a upper left sharp spot. The warm background, the cold disc, the upper right hot disc, the lower left hot disc and the sharp spot have relative emision activities of 1, 0, 1.5, 2 and 5, and diameters of 30 mm, 8 mm, 6 mm, 6 mm and 0.7 mm, respectively. Phantom 2 has 0.5 M total counts. We performed MAP reconstruction with 63×63×1 voxels of 0.7 mm×0.7 mm×0.7 mm in the field of view. The computation time was less than 1 min per 10 iteration on a DELL Precision PWS670 Workstation 3.2GHz.

Figure 3 shows the geometry of Micron-CT. This Micron-CT uses a point X-ray source with a spot size of 3 μmϕ and an X-ray CCD of Hamamatsu photonics Co. Ltd (C8800X) with×1000×1000 pixels of 8 μm width×8 μm height. Monochromatic X-rays permeating a sample are characteristic Ti -K-X-rays (4.558 keV) produced by 3MeV proton micro beams. In Our Micron-CT system, source and detectors are fixed and the sample is turned. 250 projection data are acquired par 360°, which acquisition time par 1 projection is about 8 sec. Figure 4 shows the light-microgram of a biological sample for Micron-CT, which is a ant's head of 1mmϕ. We performed OSEM (5 subset) with 456×456×360 voxels of 2.5 μm×2.5 μm×2.5 μm in the field of view. The computation time was about 12 hour per iteration on a DELL Precision PWS670 Workstation 3.2 GHz. In this case, l_{ij} was calculated when needed, because it was too much to store the intersection length l_{ij}.

RESULT AND DISCUSSION

Figure 5 shows the PET images reconstructed Phantom 1 with EM and MAP algorithm. These images are at the 30th iteration. MAP (δ=*const*) has δ and β of 875 and 100, respectively. In comparison with EM image, it is clear that the noise is strongly suppressed in the MAP images. MAP (δ=*const*) has a noise-suppression effect on only hot regions, while MAP (δ=*variable*) has a noise-suppression effect on both warm and hot regions.

Figure 6 shows the PET images reconstructed Phantom 2 with EM and MAP (δ=*variable*) algorithm. These images are at the 30th iteration. In respect of Phantom 2, MAP ($\delta=2\sigma$) was not able to reconstruct the sharp spot. So we performed the reconstruction with MAP that the value of β was set to 0.5σ. MAP ($\delta=0.5\sigma$) provided the noise suppression and the high spatial resolution. Thus it is necessary to investigate the most suitable coefficient of δ.

Figure 7 shows the CT images reconstructed the ant's head with OSEM algorithm, in which OS level is 5. These images are at the 4th iteration. With our Micron-CT, only slice with the source is acquired as complete projection data, and other slices are acquired as incomplete projection data. Nevertheless most slices were reconstructed with EM algorithm.

CONCLUSIONS

We developed an image reconstruction method for Dual Head PET and Micron-CT using EM algorithm.

MAP algorithm was applied to Dual Head PET. When the parameter δ is set to $2\sigma = 2\sqrt{voxelvalue}$, the shape of the energy function $V(r,\delta)$ is suitable for all regions. Hence it is possible to suppress the noise in both warm and hot regions on Phantom 1. On the contrary, the sharp spot was not reconstructed on Phantom 2. Thus we will study the most suitable coefficient of δ.

OSEM algorithm was applied to Micron-CT. This image reconstruction method obtains a three-dimensional image by using the cone-beam without helical scan. Most slices were well reconstructed. In addition, when data possess low statistical accuracy, the image reconstructed with EM algorithm is much improved a better Signal-to-Noise ratio in comparison with FBP. In this study, because the micro-tube of 25 μm could be reconstructed, the CT image of a cell (30 μm) will be acquired in the future.

ACKNOWLEDGEMENTS

This study was supported by 21 COE Program "Future Medical Engineering based on Bio-nanotechnology" and a Grant-in-Aid for Scientific Research (S) No. 13852017 (K. Ishii) of the Ministry of Education, Culture, Science, Sports and Technology

References

1) Feldkamp L.A., Davis L.C., and Kress J.W.,: J. Opt. Soc. Am. A. **1** (1984) 612.
2) A.Shepp L. and Vardi Y., IEEE Transactions On Medical Imaging, **MI-2** (1982) 113.
3) Lange K. and Carson R., JCAT **8** (1984) 306.
4) Hudson H.M. and Larkin R.S., IEEE Trans. Med. Imag. **13** (1994) 601.
5) Selivanov V.V., Lapointe D., Bentourkia M., and Lecomte R., IEEE Trans. Nucl. Sci. **48** (2000) 883.
6) Kontaxakis G. and Tzanakos G., Confer. Rec. IEEE Nuc. Sci. Symp. Me. Imag. Confer. **2** (1992) 1163.
7) Levitan E. and Herman G.T., IEEE Trans. Med. Imag. **MI-6** (1987) 185.
8) Moses W.W., Nucl. Instrum. Methods in Phys. Res. **A 471** (2001).
9) Rutao Y., Seidel J., Johnson C.A., Daube-Witherspoon M.E., Green M.V., Carson R.E., IEEE Trans. Med. Imag. **19** (2000).
10) Lalush D.S. and Tsui B.M.W., IEEE Trans. Med. Imag. **11** (1992) 267.
11) Ohura N., Ogawa K., and Kunieda E., Bul. Comput. Sci. Res. Center, Hosei University **13** (2000).
12) Lange K. and Fessler J.A., IEEE Trans .Med. Imag. **MI-6** (1987) 185.

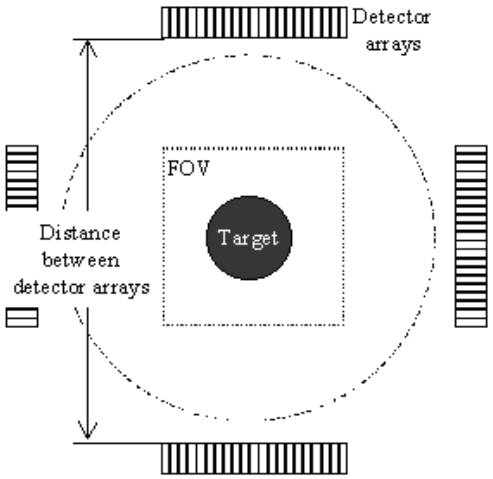

Figure 1. The simulation geometry of Dual Head PET.

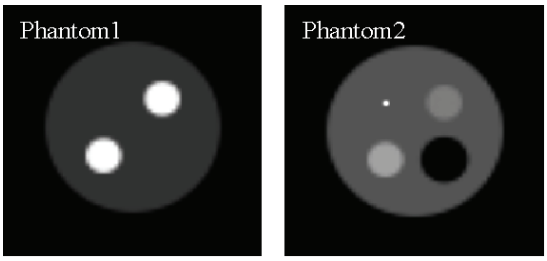

Figure 2. Digital phantoms for Dual Head PET.

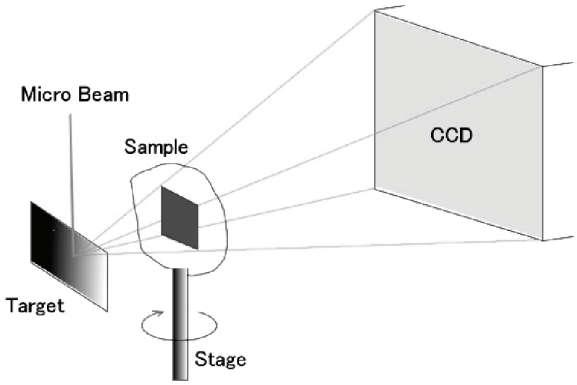

Figure 3. The geometry of Micron-CT.

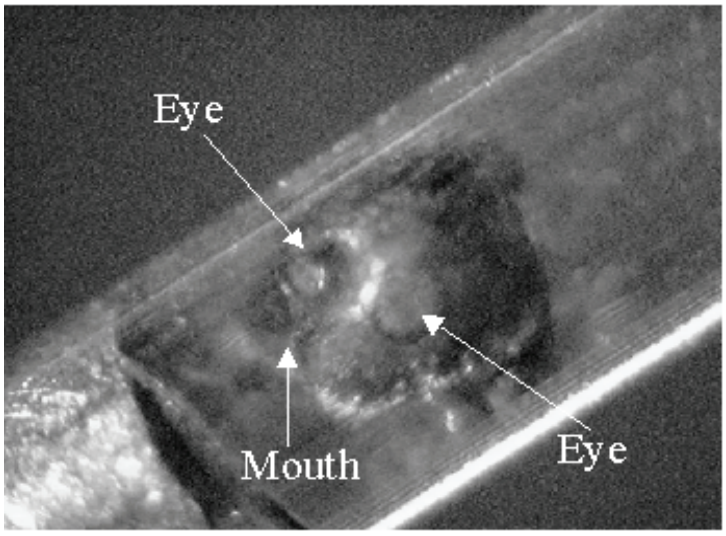

Figure 4. The biological sample (ant's head 1mmϕ) for Micron-CT.

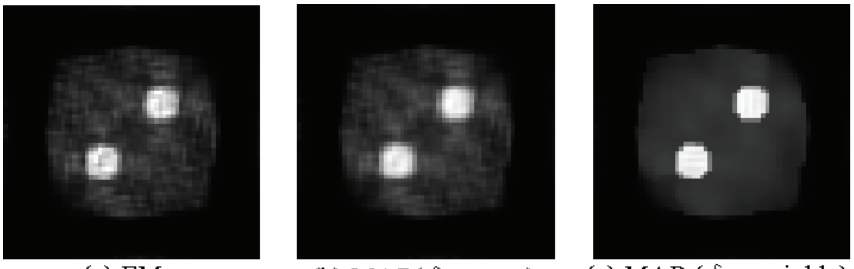

(a) EM (b) MAP(δ =const) (c) MAP (δ =variable)

Figure 5. PET reconstruction images of Phantom 1.

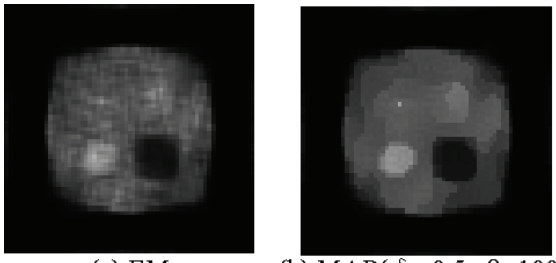

(a) EM (b) MAP(δ =0.5σ,β=100)

Figure 6. PET reconstruction images of Phantom 2.

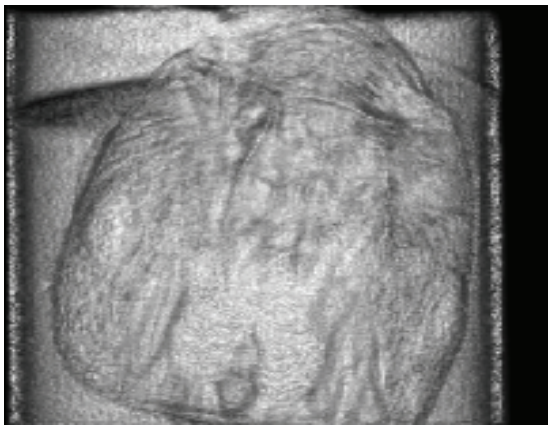

(a) The volume rendering image of the ant's head.

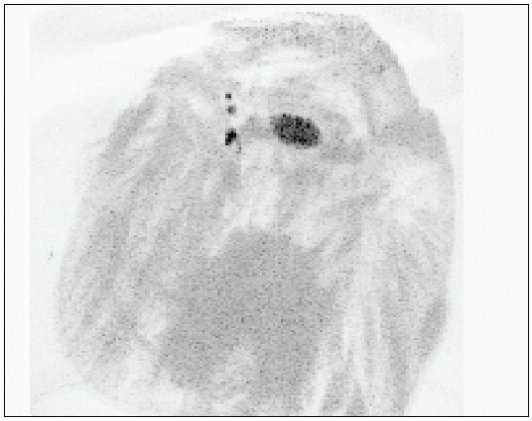

(b) The maximum intensity projection image of the ant's head

Figure 7. CT reconstruction images.